OncoTargets and Therapy

Dovepress
Taylor & Francis Group

Open Access Full Text Article

ORIGINAL RESEARCH

IGFBP1 is One of 10 Metabolic Factors Predicting Recurrence Free Survival in Gastric Cancer and Promotes Cancer Progression via ZFX-IGFBP1 Axis

Hui Liu[1,*], Yongming Huang[2,*], Guanghua Fu[3], Bo Lei[4], Ke Liu[2]

[1]Department of General Surgery, Wuhan Asia General Hospital, Wuhan, 430056, People's Republic of China; [2]Department of Gastrointestinal Surgery, Union Hospital, Tongji Medical College, Huazhong University of Science and Technology, Wuhan, 430033, People's Republic of China; [3]Department of Breast and Thyroid Surgery, the second Affiliated Hospital of Hainan Medical University, Haikou, 570311, People's Republic of China; [4]Department of Gastrointestinal Surgery, Qianjiang Central Hospital, Qianjiang, 433100, People's Republic of China

*These authors contributed equally to this work

Correspondence: Ke Liu; Bo Lei, Email unionliuke@163.com; 1260849426@qq.com

Introduction: Metabolism-related genes (MRGs) critically influence cancer prognosis, yet their role in gastric carcinoma (GC) remains poorly understood.

Methods: We analyzed 24,991 genes from 407 GC patients in TCGA to identify a metabolic gene-based prognostic signature. In vitro and in vivo functional experiments validated key findings, while transcriptional regulation mechanisms were explored through promoter interaction assays.

Results: A robust 10-metabolic gene signature was identified as strongly predictive of recurrence-free survival (RFS) in GC. Elevated insulin-like growth factor binding protein 1 (IGFBP1) expression correlated with reduced overall survival and disease-free survival. Functional studies demonstrated IGFBP1's oncogenic role in promoting GC proliferation and metastasis. Mechanistically, zinc finger protein X-linked (ZFX) activated IGFBP1 transcription by directly binding to its promoter.

Discussion: We established a prognostic nomogram integrating the 10-metabolic gene signature for GC RFS prediction. IGFBP1 emerges as a potential therapeutic target and biomarker, with ZFX-driven transcriptional activation as a novel regulatory axis in GC progression.

Keywords: nomogram, metabolic gene, gastric carcinoma, IGFBP1, ZFX

Introduction

Gastric cancer (GC) is the fourth most common type of malignant tumor globally and stands as the second leading cause of cancer-related deaths.[1–4] High death rate due to GC largely resulted from the lack of early diagnosis.[5,6] Generally, GC patients diagnosed at an advanced stage with distant metastasis, which remarkably improved cancer-related deaths.[7,8] Despite significant advances in surgical techniques, chemotherapy, and radiation therapy, the five-year survival rate for GC patients remains unsatisfactory.[9–12] Thus, the goal of this study was to unearth prognostic assessment biomarkers.

Previous researches reported that metabolic reprogramming served as a marker of cancer.[13,14] Various studies have indicated that metabolic genes were closely involved in cancer progression. For example, Sun et al proposed that the metabolic gene NR4A1 could serve as a promising therapeutic target for non-smoking female individuals diagnosed with non-small cell lung cancer.[15] Nwosu ZC et al suggested that liver cancer cell lines remarkably mimicked the metabolic gene expression pattern of the related human tumors.[16] Na KJ et al indicated that tumor metabolic features identified by ^{18}F-FDG PET were associated with gene networks of immune cell microenvironment in head and neck carcinoma.[17] An accumulating number of studies have found that metabolic genes may be underlying prognostic markers of cancers. For instance, Yao L et al reported that high expression of metabolic enzyme PFKFB4 was related to poor prognosis of operable breast cancer.[18] Gajjar KK et al demonstrated that a robust correlation between the activity of 5-fluorouracil

Received: 4 November 2024
Accepted: 24 May 2025
Published: 5 June 2025

metabolizing enzymes and both prognosis and treatment response in patients diagnosed with colorectal cancer.[19] Nevertheless, currently, fewer studies have confirmed the power of metabolism-related gene for predicting the prognosis of GC. Given their prognostic potential in GC, the power of the metabolic genes for predicting the prognosis of GC should be explored in depth.

In recent years, the dual roles of IGFBP1 in gastric cancer have gradually been unveiled. Existing studies have demonstrated that IGFBP1 not only serves as a prognostic marker but also promotes gastric cancer metastasis and metabolic abnormalities through mechanisms such as regulating the reactive oxygen species (ROS) pathway, and interacting with gut microbiota.[20,21] However, the upstream regulatory mechanisms of IGFBP1 in gastric cancer and its synergistic effects with other metabolic genes remain unclear. Additionally, despite the widely recognized importance of metabolic genes in cancer prognosis, a comprehensive prognostic model based on metabolic genes for gastric cancer still urgently requires development. In this study, by integrating multi-omics data, we constructed, for the first time, a prognostic marker based on 10 metabolic genes and uncovered a novel mechanism whereby ZFX activates IGFBP1 transcription by directly binding to its promoter. This finding not only refines the regulatory network of IGFBP1 but also provides potential therapeutic targets for the precise treatment of gastric cancer.

Materials and Methods

Data Downloading and Processing

This was a retrospective research using TCGA data by 'TCGAbiolinks' package[22] and GEO database via 'GEOquery' package[23] for comprehensive analysis. For all data-sets, our research only selected samples with complete RFS information. Totally, 24991 genes and 384 patients with GC were available for analysis. Metabolic-associated genes were extracted through metabolic pathway website (http://www.bmrb.wisc.edu/data_library/Genes/Metabolic_Pathway_tablehtml). Finally, 2059 metabolic genes and 384 patients with GC were identified for univariate Cox regression analysis. What's more, GSE26253 dataset and corresponding clinical information were employed as external validation dataset which was obtained from GEO database using GEO query package. Furthermore, our study seeks to perform data mining and analysis utilizing the TCGA and GEO databases, human tissue study was approved by the Institutional Review Board of Tongji Medical College. All procedures were undertaken in accordance with guidelines set forth by the Declaration of Helsinki.

Statistical Analysis

Initially, we screened the metabolic genes by including those genes correlated with GC patients' RFS ($P<0.05$) using univariate Cox regression analysis. The candidate metabolic genes strongly relevant to RFS were then determined by LASSO analysis. We selected 33 candidate metabolic genes of the greatest importance to conduct multivariable Cox's analysis (backward and forward stepwise method). Finally, a 10-metabolic gene signature were identified for the prediction of GC patients' RFS based on multivariable Cox's analysis. 384 samples, the training set and internal validation set were randomly assigned. The prognostic biomarker model was constructed with a training set containing 269 samples and validated by using a testing set containing 115 samples. The coefficient of multivariable Cox regression analysis was used to establish the metabolic gene risk scoring formula, and the RFS risk score of each patient was calculated. Patients with risk scores larger than the median were divided to the high-risk cohort, meanwhile the others were divided to the low-risk cohort. In addition, the 10-metabolic gene signature were subjected to ROC analysis to weigh the capacity of predicting GC patients' RFS the Kaplan-Meier analysis was conducted on the internal validation dataset, external validation dataset, and the entire TCGA dataset to evaluate the effectiveness of the 10-metabolic gene markers. All ROC curves and Kaplan-Meier survival analyses were performed utilizing the R programming (version 4.2.1). RFS are defined as time to tumor recurrence, distant metastasis, or all-cause death confirmed by pathology or imaging. Patients without events were truncated at the last follow-up.

For laboratory experiments, statistical analyses were performed using GraphPad Prism (version 7.0, GraphPad Software, Inc., La Jolla, CA, USA). The data was presented as the mean ± standard deviation (SD), the error bars are standard deviations, and significance testing was conducted using a two-tailed Student's *t*-test and a one-way analysis of variance (ANOVA). To ensure reliability, the experiments were independently replicated at least three times. Statistical significance was considered when $P < 0.05$.

Quantitative Reverse Transcription-Polymerase Chain Reaction (qRT-PCR)

The GC tissues were subjected to RNA extraction using TRIzol® reagent (Thermo Fisher Scientific, Inc) according to the manufacturer's protocol. Subsequently, reverse transcription was performed utilizing the PrimeScript™ RT reagent Kit (Takara Bio, Inc)., followed by qRT-PCR using SYBR Green Real-Time PCR Master Mixes (Applied Biosystems). The expression levels of mRNA were determined using the $2^{-\Delta\Delta Cq}$ method and normalized against GAPDH. The primer sequences can be found in Table S1.

Construction of the Nomogram

The univariate Cox proportional hazard analysis and multivariable Cox proportional hazard analysis were implemented across risk score and a few clinicopathological factors. The factors for which yielded a $P \leq 0.05$ in multivariable Cox proportional hazard analysis were employed for establishing the nomogram according to the 'rms' R package. The predictive robustness for GC prognosis of the nomogram was tested through calibration plots, ROC, C-index decision curve analysis (DCA). The outcome of the nomogram was exhibited with a calibrate curve and the 45-degree line stood for a perfect predicting ability. The DCA aims to evaluate the clinical efficacy of risk stratification strategies based on predictive models (such as more intensive monitoring of high-risk patients), rather than directly comparing specific treatment approaches. The calculation of net benefit is based on the trade-off between avoiding excessive intervention in low-risk patients (reducing unnecessary examinations) and effectively managing high-risk patients (early detection of recurrence).

Cell Culture

The human normal gastric mucosal epithelial cell line (GES-1) and gastric cancer cell lines (MNK45, SGC7901, AGS, and BGC823) were obtained from the Cell Bank of Type Culture Collection Committee at the Chinese Academy of Sciences (Shanghai, China). All cells were cultured using Roswell Park Memorial Institute (RPMI) 1640 medium (Gibco, Grand Island, NY, USA), supplemented with 10% fetal bovine serum (FBS), 1% penicillin, and streptomycin. The cells were then incubated in a CO_2 incubator set at a temperature of 37°C.

Chromatin Immunoprecipitation (CHIP)

The EZChIP™ Chromatin Immunoprecipitation Kit was utilized to conduct chromatin immunoprecipitation (ChIP) assays, following the protocol provided by the manufacturer. In brief, MNK45 and AGS cells were subjected to crosslinking with 1% formaldehyde for a duration of 10 minutes at room temperature. Subsequently, inactivation of the crosslinking was achieved using 125 mm glycine. The target cells were then collected and sonicated to generate fragments measuring approximately 200 bp in length. For immunoprecipitation, an anti-ZFX antibody or control IgG was employed.

Cell Proliferation Assay

The Cell Counting Kit-8 (CCK-8; Dojindo Laboratories, Japan) was employed for the evaluation of cell proliferation. Cells were seeded at a density of 1×10^3 cells per well in 96-well plates. Following 1, 2, 3, 4, and 5 days of cell culture, each well received the addition of 10 μL CCK-8 solution and underwent incubation for a duration of 2 hours at a temperature of 37°C. Subsequently, the absorbance was measured at a wavelength of 450 nm using a microplate reader (Thermo Fisher Scientific, Waltham, MA, USA).

Cell Invasion and Migration Assays

To perform the migration assay, MNK45 and AGS cells were transfected with recombinant plasmids for 72 hours. Subsequently, these cells were placed in the upper chamber of a Transwell system (Corning, Rochester, NY, USA) at a density of 1×10^5 cells per well in serum-free medium. For the invasion assay, the upper chamber was pre-coated with Matrigel (BD Biosciences, Franklin Lakes, NJ, USA), followed by mirroring the remaining steps from the migration assay. A fresh medium containing 20% FBS was then added to the lower chamber. The cells were incubated at 37°C under 5% CO_2 for 24 hours. After incubation, fixation was performed using 4% paraformaldehyde (PFA), staining was

carried out using 0.5% crystal violet (Sigma-Aldrich, USA) for approximately 20 minutes and finally imaged using an Olympus IX71 microscope (Japan).

Cell Cycle and Apoptosis Analysis

A density of 2×10^5 cells per well was used to seed the cells in 6-well plates. To analyze the cell cycle, MKN45 and AGS cells were treated with siRNAs for 48 hours, followed by overnight fixation in 70% ethanol at −20 °C. The fixed cells were then stained with phycoerythrin and subjected to flow cytometry for cell cycle distribution analysis. For the apoptosis assay, a total of 10^5 cells were collected and washed twice with ice-cold PBS. The cells were resuspended in binding buffer, treated with Annexin V-FITC and 7-AAD (BD Biosciences), and incubated in darkness for 15 minutes. Flow cytometry analysis was performed within 1 h to measure Annexin V-FITC positive cells (BD FACVerse).

Cell Transfection

The cells were cultured in 6-well plates with a density of 2×10^4 cells per well and then transfected with recombinant plasmids (GenePharma, Shanghai, China) using Lipofectamine 3000 (Invitrogen, Carlsbad, CA, USA) for a duration of 12 hours according to the manufacturer's instructions. Before proceeding with further experiments, we evaluated the effectiveness of gene knockdown or overexpression through qRT-PCR and Western blot analysis.

shRNA Interference

The shRNA used in this study was obtained from Sigma-Aldrich. Subsequently, the shRNA plasmid, along with pVSV-G and pEXQV, was introduced into 293T cells using Lipofectamine 3000. Following a 24-hour incubation period after transfection, the culture medium was replaced with fresh Dulbecco's Modified Eagle Medium (DMEM) supplemented with 1 mm sodium pyruvate. Two days post-transfection, the supernatant containing the shRNA virus was collected and co-cultured with MKN45 and AGS cells for a duration of 24 hours. After this co-culture period, infected cells were selected by adding puromycin at a concentration of 1 mg/mL.

Western Blot Analysis

The harvested cells were subjected to treatment with lysis buffer containing 1% protease inhibitor and phosphatase inhibitor, followed by cell lysis on ice for a duration of 15 minutes. To obtain proteins, the resulting cell lysate was centrifuged at 12,000 g for 15 minutes at a temperature of 4°C. The supernatant was then utilized for protein concentration measurement using a Protein Quantification Kit (#P0012S, Beyotime Biotechnology). Equal quantities of total protein were loaded into individual wells of an SDS-PAGE gel and subsequently transferred onto a PVDF membrane. At room temperature, the membrane was blocked with skimmed milk (5%) for a period of 60 minutes. Following this step, primary and secondary antibodies were incubated separately with the membrane overnight at a temperature of 4°C and for one hour at room temperature respectively. Finally, to visualize protein bands using X-ray film, ECL detection reagent (#WP20005, Thermo Fisher Scientific) was applied onto the surface of the membrane. Antibody information: anti-IGFBP1 (13,981-1-AP, Proteintech), anti-PTEN (60300-1-Ig, Proteintech), anti-pAKT (28731-1-AP, Proteintech), anti-AKT (10176-2-AP, Proteintech), anti-ZFX (27655-1-AP, Proteintech), anti-GAPDH (10494-1-AP, Proteintech), HRP-conjugated Goat Anti-Rabbit IgG (SA00001-2, Proteintech), HRP-conjugated Goat Anti-Mouse IgG (SA00001-1, Proteintech).

Animal Study

Ten male BALB/c nude mice at the age of 6 weeks were obtained from Beijing Weitong Lihua Experimental Animal Technology Co., Ltd. These mice were divided randomly into two groups, with each group consisting of five mice. Tumor cells were injected individually into the right dorsal side of each mouse in a random and blinded manner. A total of five mice received 1×10^6 cells per mouse. The longitudinal and transverse dimensions of the tumors were measured every 5 days using a vernier caliper. Tumor volume (V) was calculated using the formula: $V = 0.5 \times D \times d^2$, where D represents the longitudinal dimension and d represents the transverse dimension. On day 25 after injection, euthanasia was performed on all mice and tumor tissues were weighed. The mice were housed in sterile cages that were free from

pathogens. All animal experiments were carried out in accordance with NIH Guidelines for the Care and Use of Laboratory Animals and approved by the Animal Care Committee of Tongji Medical College.

Luciferase Reporter Assay

The potential targeting association between ZFX and IGFBP1 was predicted by the JASPAR software, which was subsequently validated through luciferase reporter gene assays. MNK45 and AGS cells were transfected with PMIR-REPORT luciferase vectors containing either wild-type (WT)- ZFX-3'UTR or mutant (MUT)-ZFX-3'UTR, in addition to shRNA specifically targeting IGFBP1 or a negative control (NC) shRNA. Following 48 hours of incubation, the cells were collected, and luciferase signals were quantified using the TECAN Infinite F500 platform and the Dual-Luciferase Reporter Assay System according to the manufacturer's instructions. To ensure reproducibility, this experiment was repeated at least three times.

Results

Clinical Characteristics of the GC Patients in This Study

To explore underlying roles of metabolic genes in GC, totally, 2059 metabolic genes and 384 GC patients were extracted from TCGA data. Table S2 summarized clinicopathological features of all the selected GC patients in TCGA databases. Figure 1A summarized the study flowchart.

Construction of the Prognostic Signature

We conducted an analysis using both univariate Cox regression and LASSO Cox regression to examine the associations between 2059 metabolic genes and RFS in patients with GC (Table S3). From the LASSO Cox regression analysis, we identified 33 metabolic genes that were closely associated with RFS in GC patients (Figure 1B and C). Ultimately, through multivariable Cox analysis, 10 metabolism-related genes (ALG2, DCT, IGFBP1, PSAT1, YWHAG, PAX8, HADH, F7, FAAH) were significantly implicated in the RFS of GC patients (Figure 1D). The risk score was calculated as follows: Risk score = −0.00268*ALG2 + 0.05124*DCT + 0.01748*HAMP + 0.00141*IGFBP1 - 0.00169*PSAT1 + 0.00044*YWHAG + 0.00266*PAX8 - 0.00144*HADH + 0.00482*F7 - 0.00476*FAAH. These 10 metabolic gene signatures were utilized to predict the RFS of GC patients.

Correlation Between the 10-Metabolic Gene Signature and Patients' RFS Based on Kaplan-Meier Analysis

Next, the patients with gastric cancer were divided into two groups (high-risk and low-risk) according to the median risk score value. The disparity in RFS between these two cohorts was examined using the Kaplan-Meier analysis. In the internal validation set, the GC patients with low-risk scores demonstrated a significantly superior RFS compared to those with high-risk scores (P = 5e-05) (Figure 2A). Similar results were observed in the external validation dataset (P = 0.004) (Figure 2C) and across the entire TCGA dataset (P = 3e-13) (Figure 2E).

Validation of the Predictive Power of the 10-Metabolic Gene Signature Using ROC Analysis

The predictive robustness of the 10 metabolic gene signatures was assessed by means of time-dependent ROC curves. In the internal validation dataset, the area under the curve (AUC) for the 10 metabolic gene signatures at 1, 3, and 5 years was (0.803, 0.789, 0.800), respectively (Figure 2B). The external validation dataset also demonstrated a strong predictive power, with respective values of 0.735, 0.804, and 0.765 (Figure 2D). Furthermore, this high predictive power was consistently observed across the entire dataset, with respective values of 0.770, 0.797, and 0.761 (Figure 2F). We found that the 10 metabolic gene signatures serve as robust predictors of RFS in GC patients. Subsequently, we ranked the samples based on their risk scores (Figure 2G). Furthermore, a dot plot was generated to depict their survival status (Figure 2H), revealing that the high-risk cluster exhibited a generally unfavorable survival profile compared to the low-risk cluster. Figure 2I displays a heatmap of the 10 metabolic genes grouped by risk score, which aligns with the previous boxplots. Comparable findings were also noted in

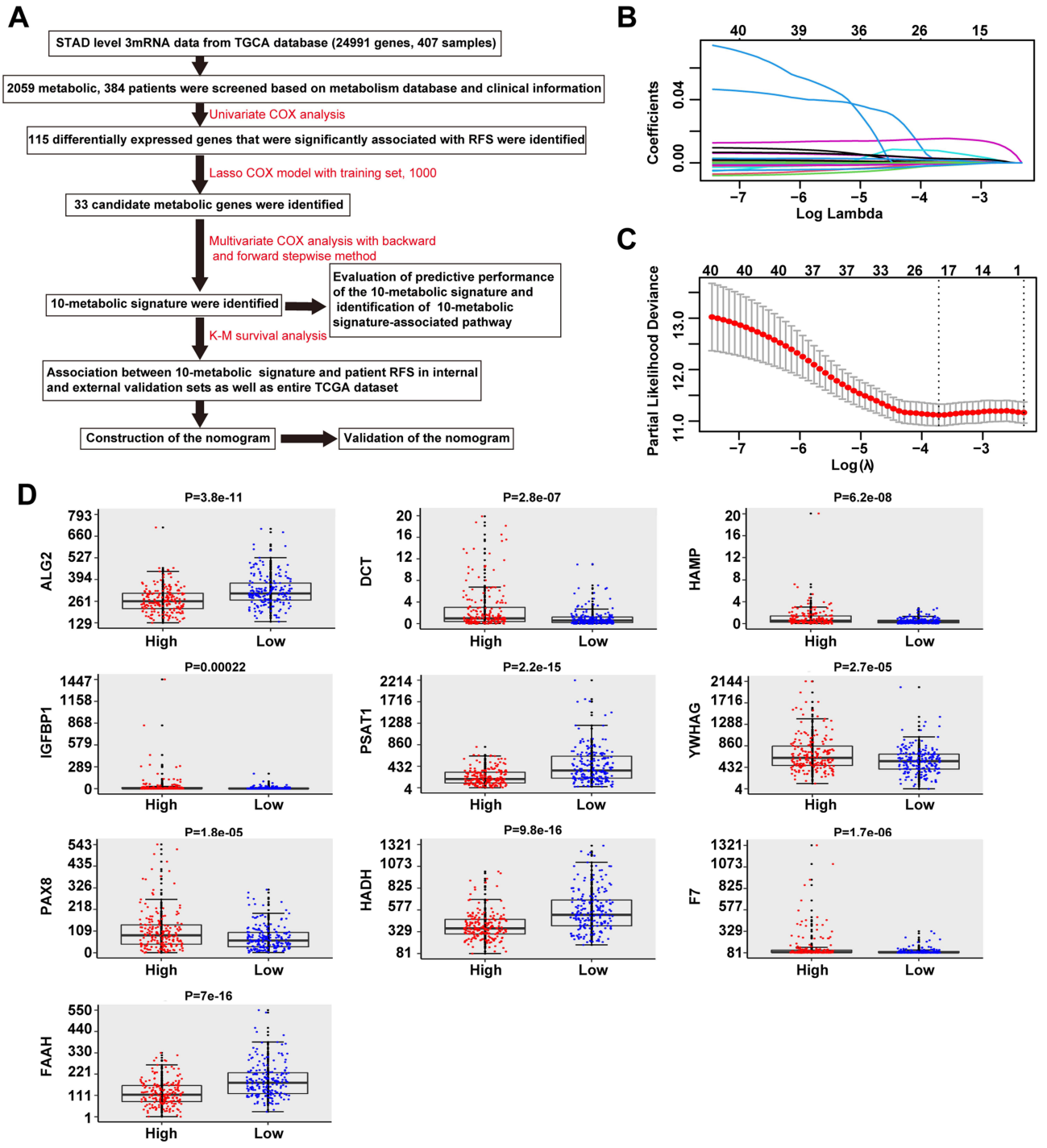

Figure 1 Prediction and identification of metabolic genes associated with RFS in GC patients. (**A**) Research design and flowchart. (**B**) In the LASSO model, 10-fold cross-validation was performed using the minimum criteria (ie, 1-SE criteria) to select the optimal tuning parameter. (**C**) Distribution plot of LASSO coefficients for 99 metabolic genes. The coefficient distribution plot was generated based on the logarithmic (lambda) sequence. A vertical line is depicted at the optimal lambda value selected through 10-fold cross-validation, resulting in 33 non-zero coefficients. (**D**) Box plots of the expression levels of 16 metabolic genes in risk cohorts in the TCGA dataset. We divided GC patients into two cohorts (high-risk and low-risk) based on the median risk score value. "High" and "Low" refer to the high-risk and low-risk cohorts, respectively. The Mann–Whitney *U*-test was used to assess the difference between the two cohorts, and the P-value indicating statistical significance of this difference is displayed on the graph.

the GSE26253 dataset (Figure S1). Following this, we conducted subgroup analyses on several clinical variables, including age, gender, metastasis status, anatomical location, stage, and histological type. In most subgroups, the 10 metabolism-related gene signatures demonstrated good predictive ability (Figure S2-S8).

https://doi.org/10.2147/OTT.S499695

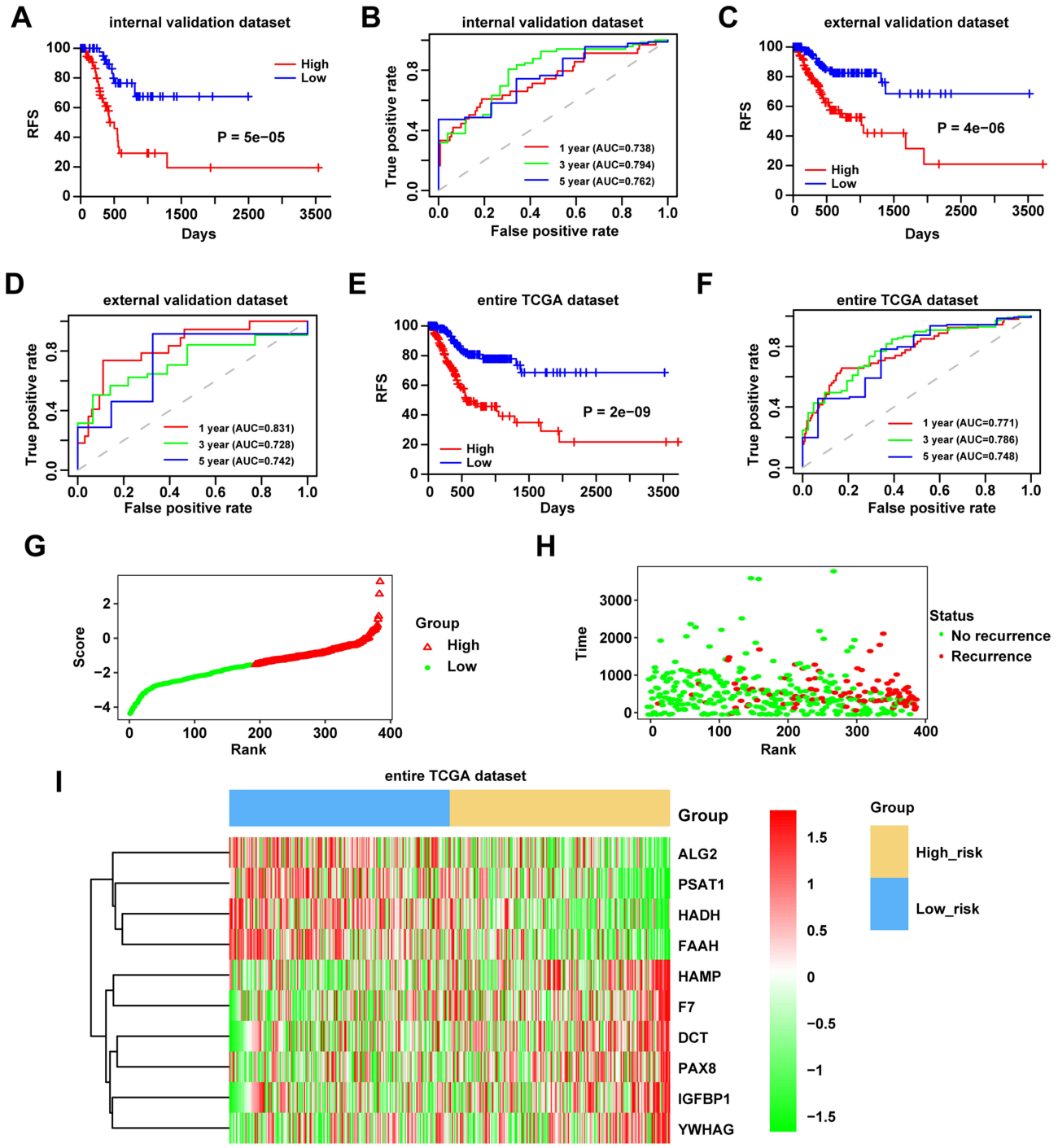

Figure 2 Kaplan-Meier survival curves and receiver operating characteristic (ROC) curves for GC patients in the internal validation set, external validation set, and the entire dataset. (**A, C** and **E**) Kaplan-Meier survival curves for the internal dataset, external dataset, and the entire TCGA dataset, respectively. Gastric cancer patients were divided into high-risk and low-risk groups using the median score as the cutoff. The time unit on the horizontal coordinate is days. The Kaplan-Meier analysis with a two-sided Log rank test was used to assess the difference in relapse-free survival (RFS) between low-risk and high-risk GC patients. (**B, D** and **F**) ROC curves for the internal dataset, external dataset, and the entire TCGA dataset, respectively. One-year, three-year, and five-year ROC curves for the 10 metabolic gene signatures were utilized to demonstrate their value in predicting RFS for GC patients. A higher AUC value indicates better performance of the ROC curve. (**G**–**I**) Analysis of metabolic gene risk scores for 384 GC patients in the TCGA dataset. (**G**) Relationship between metabolic gene risk score distribution and risk score ranking. The median risk score serves as the cutoff point. Red triangles represent the high-risk group, and green circles represent the low-risk group. (**H**) Survival status of GC patients. Red circles indicate the high-risk group, and green circles indicate the low-risk group. (**I**) Heatmap of the expression profiles of 10 metabolic genes in GC patients. Each row of the heatmap represents a metabolic gene signature, and each column represents a GC patient. Differences in the scores of each metabolic gene signature between the high-risk and low-risk groups can be observed from the heatmap.

https://doi.org/10.2147/OTT.S499695

Development and Validation of Nomograms for Predicting Prognosis of GC Patients

The observed hazard ratios (HRs) indicate a significant correlation between the 10 metabolic gene signatures and RFS in patients with GC (P<0.001, HR 2.16, 95% CI 1.72–2.57) (Table S4), suggesting that this signature shows potential as a prospective predictor of RFS in individuals diagnosed with GC. Furthermore, we developed a nomogram to effectively and quantitatively predict RFS in GC patients (Figure 3A). The significance between the 10-metabolic-based factor and the conventional clinic-associated covariates was described in Figure 3B. The results indicate that the C-index (0.809, 95% CI: 0.763–0.837), AUC (at 1-year, 3-year, and 5-year intervals: 0.875, 0.924, and 0.876) (Figure 3B and C), as well as the calibration plots all exhibited favorable performance (Figure 3D–F). Additionally, when the threshold probability is about 0.03–0.77, it was observed that the nomogram exhibited better clinical usefulness in predicting RFS in patients

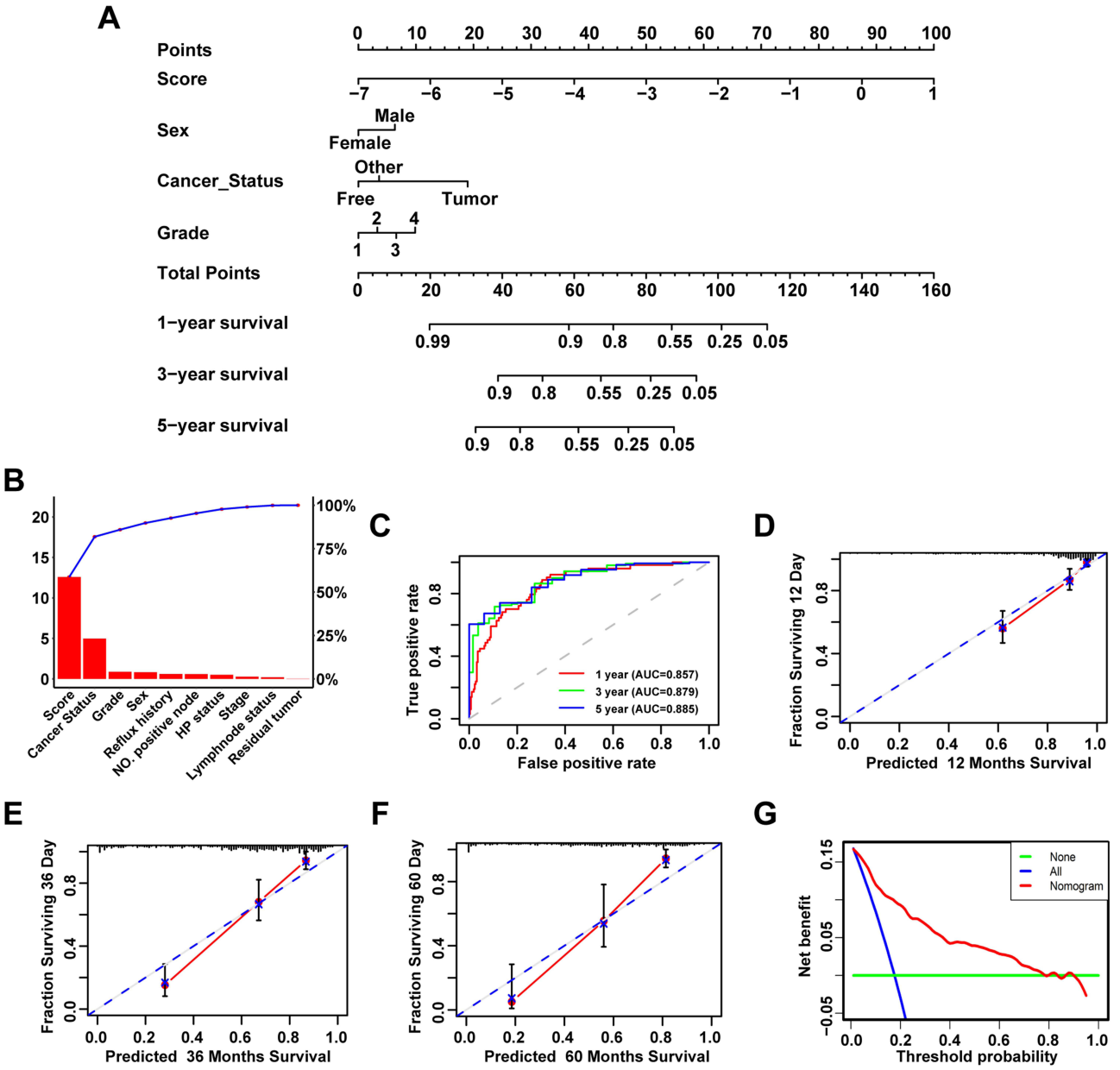

Figure 3 Identification of the 10-metabolic gene signature-relevant signaling pathways. (**A**) The nomogram was developed in the entire TCGA cohort, with the risk score, sex, cancer status and tumor grade. (**B**) The higher the bar chart, the greater the weight and importance it indicates. (**C**) Depict the 1-year, 3-year, and 5-year ROC curves of the metabolic gene-related nomogram in GSE26253 cohort. (**D**–**F**) Represent the calibration curves of the nomogram at 12 months, 36 months, and 60 months, respectively. The closer the dashed line is to the ideal line, the better the predictive ability of the nomogram. (**G**) DCA of the nomogram, plotting the net benefit against the threshold probability. The red line represents the nomogram, the blue line represents the treat-all strategy, and the green line represents the treat-none strategy.

https://doi.org/10.2147/OTT.S499695

with GC compared to strategies of treating all or treating none (Figure 3G). Consequently, the nomogram possesses considerable worth and demonstrates encouraging prospects for practical application in clinical settings.

IGFBP1 Is Upregulated in Both GC Cells and Tissues

Next, we analyzed the ability of metabolism-related genes to predict overall survival (OS) and RFS in GC based on TCGA-STAD RNA-seq data. The results indicated that the cluster with a higher risk showed considerably reduced OS and RFS compared to the cluster with a lower risk. (Figure 4A and B). Among the 10 metabolic genes, IGFBP1 expression was most upregulated in TCGA gastric cancer tissues (Figure 4C and D). Besides, compared to GES-1 cells, the mRNA expression levels of IGFBP1 were elevated in AGS, MNK45, SGC7901, and BGC823 cells, with particularly notable increases in AGS and MNK45 (Figure 4E). Similar results were obtained in collected tumor tissue compared adjacent normal tissue (Figure 4F). Furthermore, we evaluated the expression of IGFBP1 in GC tissues using immunohistochemistry (IHC) assay for Human Protein Atlas (HPA) database. The findings revealed a notable increase in the expression levels of IGFBP1 in GC tissues compared to non-tumor tissues (Figure 4G), suggesting the potential significance of IGFBP1 in driving the advancement of gastric cancer.

IGFBP1 Promotes the Progression of GC Cells

To further elucidate the role of IGFBP1 in gastric cancer, we employed two shRNAs to downregulate the expression of IGFBP1 in MNK45 and AGS cells. First, the efficiency of IGFBP1 knockout in the aforementioned cell lines was verified by qRT-PCR (Figure 5A). Meanwhile, downregulating IGFBP1 expression resulted in a reduction of proliferation marker pAKT and elevation of cancer-inhibiting marker PTEN in MNK45 and AGS cells (Figure 5B). Besides, the inhibition of cell proliferation and colony formation in MNK45 and AGS cells was observed upon downregulation of IGFBP1 (Figure 5C and D). Additionally, the migratory and invasive capacities of GC cells were significantly attenuated when the expression of IGFBP1 was suppressed, as demonstrated by transwell assays (Figure 5E and F).

Flow cytometry was employed to analyze the cell cycle distribution and apoptosis in MKN45 and AGS cells transfected with shIGFBP1 or shControl. The results showed that compared to the shControl group, both cell types demonstrated a reduced proportion of cells in the S phase and an elevated apoptosis rate (Figure 6A and B). Overall, these findings indicate that IGFBP1 knockdown can induce cell cycle arrest and promote apoptosis in MKN45 and AGS cells. Furthermore, we conducted an investigation to assess the impact of IGFBP1 on tumor growth in vivo by establishing a subcutaneous xenograft model. The results demonstrated a significant reduction in both the size and weight of tumors upon depletion of IGFBP1 (Figure 6C). These findings provide compelling evidence regarding the pivotal role played by IGFBP1 in driving the progression of gastric cancer cells.

ZFX Regulates IGFBP1 Expression by Binding to the Promoter Region of IGFBP1

To investigate the upstream regulators of IGFBP1, we employed the JASPAR database as a bioinformatics tool to predict the TFs that potentially govern the expression of IGFBP1, with a specific focus on identifying putative targets. As a result, four candidates were successfully identified. Next, we performed qRT-PCR analysis to evaluate the mRNA expression levels of the transcription factors ZFX, KLF15, SP1, and SP4 in GES1, MKN45, and AGS cell lines. The findings revealed that ZFX mRNA expression levels exhibited the most significant elevation in comparison to all other examined transcription factors (Figure 7A). Furthermore, overexpression of ZFX in MKN45 and AGS cells led to an increase in IGFBP1 expression levels (Figure 7B and C). Interestingly, the CCK-8 and transwell assays demonstrated that the overexpression of ZFX significantly enhanced the proliferative and migratory capacities of MKN45 and AGS cells. Nevertheless, when IGFBP was suppressed, the tumor-promoting effect induced by ZFX was abolished. (Figure 7D-7F). Next, we utilized bioinformatic algorithms to predict the potential interaction sites between ZFX and the IGFBP1 gene and listed the mutated sequences in the MUT vector (Figure 7G). Subsequently, CHIP assay validation experiments demonstrate that ZFX exhibits a robust binding affinity to IGFBP promotor in MKN45 and AGS cells (Figure 7H). As shown in Figure 7I, the overexpression of ZFX in MNK45 and AGS cells significantly enhanced the luciferase activity in the WT IGFBP promoter. However, when IGFBP knockdown was performed, these effects were nearly abolished. These findings suggest that ZFX directly regulates both the expression and activity of IGFBP within gastric cancer cells.

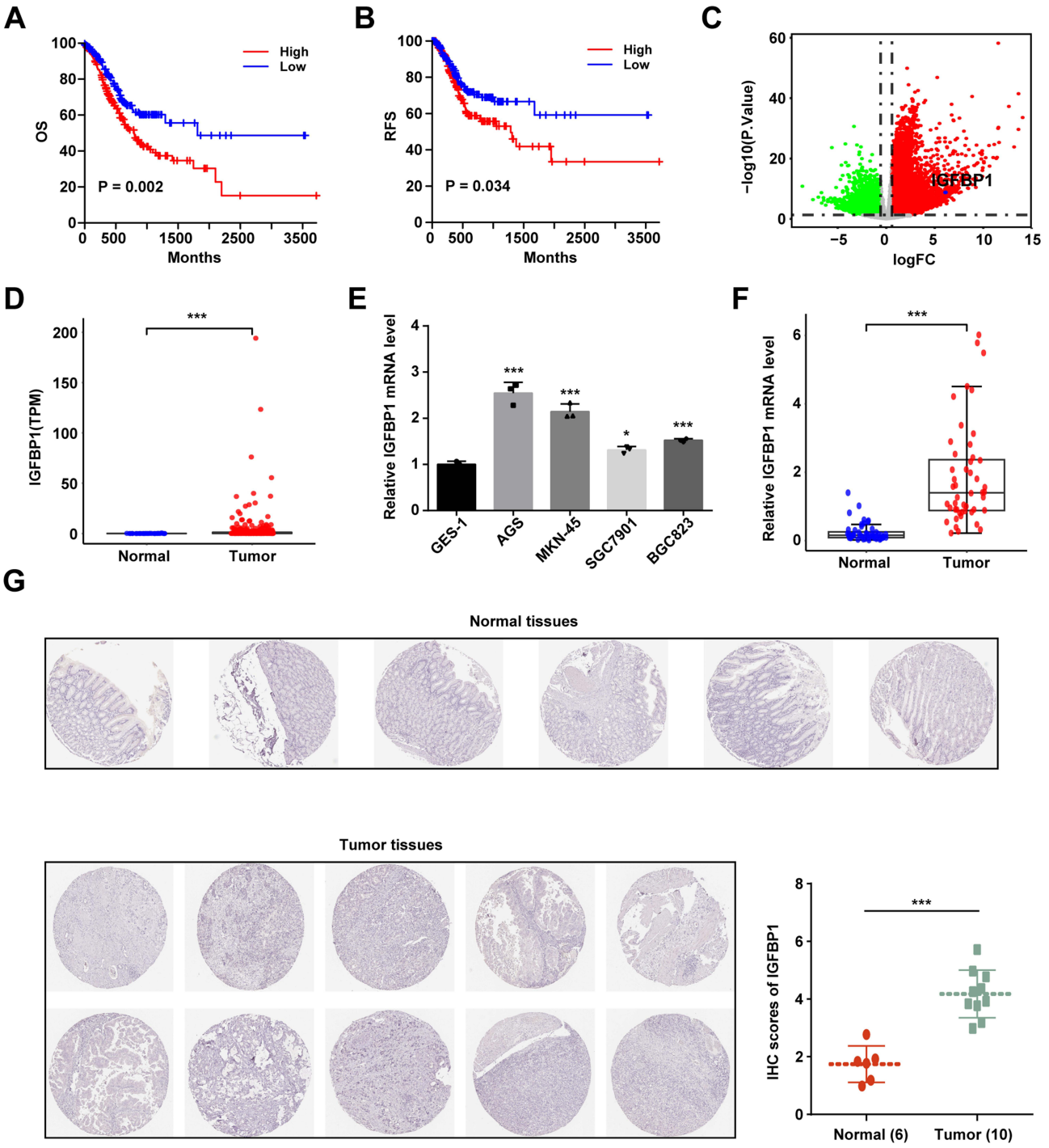

Figure 4 Clinicopathological Characteristics of IGFBP1 in GC. (**A** and **B**) Kaplan-Meier survival analysis based on TCGA-STAD RNA-seq data for OS (**A**) and RFS (**B**) in GC patients stratified into high-risk and low-risk groups, with P-values indicated. (**C**) The TCGA-STAD dataset is visualized in a volcano plot, highlighting genes exhibiting differential expression. Upregulated and downregulated genes are depicted by red and green dots respectively, while IGFBP1 is specifically emphasized as a blue dot. (**D**) Expression values of IGFBP1 in adjacent non-tumor and tumor tissues from the TCGA-STAD dataset. (**E**) Evaluation of IGFBP1 gene expression in GES-1, AGS, MNK45, SGC7901, and BGC823 cells by qRT-PCR. Data are presented as the average ± standard deviation (SD) obtained from at least three separate trials. (**F**) Analysis of IGFBP1 mRNA expression levels in collected gastric cancer samples. (**G**) Immunohistochemical (IHC) analysis of IGFBP1 protein levels in tissue microarrays (n = 5 normal tissues, n = 10 gastric cancer tumor tissues). Data are presented as mean ± SD. *P<0.05, ***P<0.001.

Discussion

GC is a pivotal malignancy and ranks as the fifth most prevalent carcinoma globally.[24] The incidence of GC-related death is high mainly due to the lack of early diagnosis.[5,6] Despite advancements in surgical techniques, chemotherapy regimens, and

 https://doi.org/10.2147/OTT.S499695

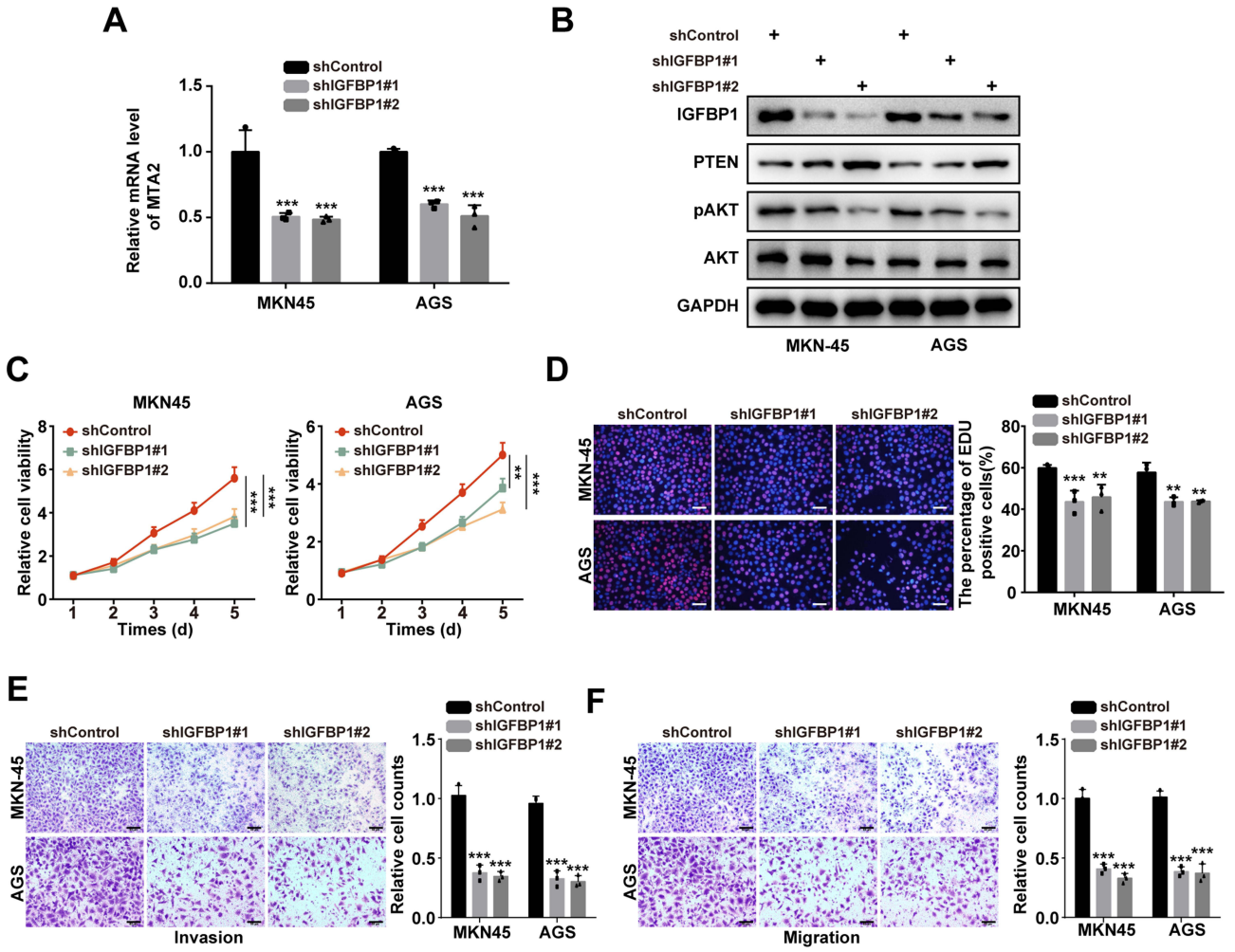

Figure 5 The effects of IGFBP1 on proliferation, invasion, and migration of gastric cancer (GC) cells. (**A** and **B**) Expression of IGFBP1 in MKN45 and AGS cells treated with indicated short hairpin RNAs (shRNAs) was detected by real-time quantitative polymerase chain reaction (RT-qPCR) **(A)** and Western blot analysis (**B**). Data were reported as the mean ± standard deviation (SD) from at least three independent trials. (**C** and **D**) Proliferation ability of MKN45 and AGS cells was assessed by cell viability (**C**) and EdU assays (**D**). Data were reported as the mean ± standard deviation (SD) from at least three independent trials. (**E** and **F**) Invasion and migration capabilities of MKN45 and AGS cells with indicated shIGFBP1 were explored using Transwell assays. Data were reported as the mean ± standard deviation (SD) from at least three independent trials. **P<0.01, ***P<0.001.

radiotherapy methods, the 5-year survival rate for patients diagnosed with GC remains unsatisfactory.[25] Thus, the aim of our study was to discover prognostic assessment markers in GC.

In this study, we discovered a combination of 10 metabolism-related genes (ALG2, DCT, IGFBP1, PSAT1, YWHAG, PAX8, HADH, F7, FAAH, HAMP) and effectively predicted the RFS in patients diagnosed with GC through the utilization of univariate Cox proportional hazard analysis, LASSO Cox regression analysis and multivariable Cox proportional hazard analysis. Furthermore, we employed both internal and external validation datasets to assess the effectiveness of our 10-gene metabolic signature. Additionally, we present novel evidence demonstrating the significance of IGFBP1 as a crucial molecular prognostic factor, correlating with reduced overall survival and disease-free survival in GC patients. Subsequent functional experiments revealed that IGFBP1 promotes invasion, migration and induced cell apoptosis in GC cells. Our study further uncovered that ZFX could bind to the promotor of IGFBP1, thereby inducing its upregulated expression and ultimately facilitating the progression of GC. In summary, our study demonstrates that IGFBP1 as a MRGs contributes to GC development.

Numerous researchers have discovered that the above-mentioned 10 metabolic genes were strongly correlated with cancer progression. For instance, Chai et al revealed that PAX8 was a potential biomarker for the diagnosis of primary epithelial ovarian cancer.[26] Du et al demonstrated the utilization of a co-loaded thermosensitive liposome system

https://doi.org/10.2147/OTT.S499695

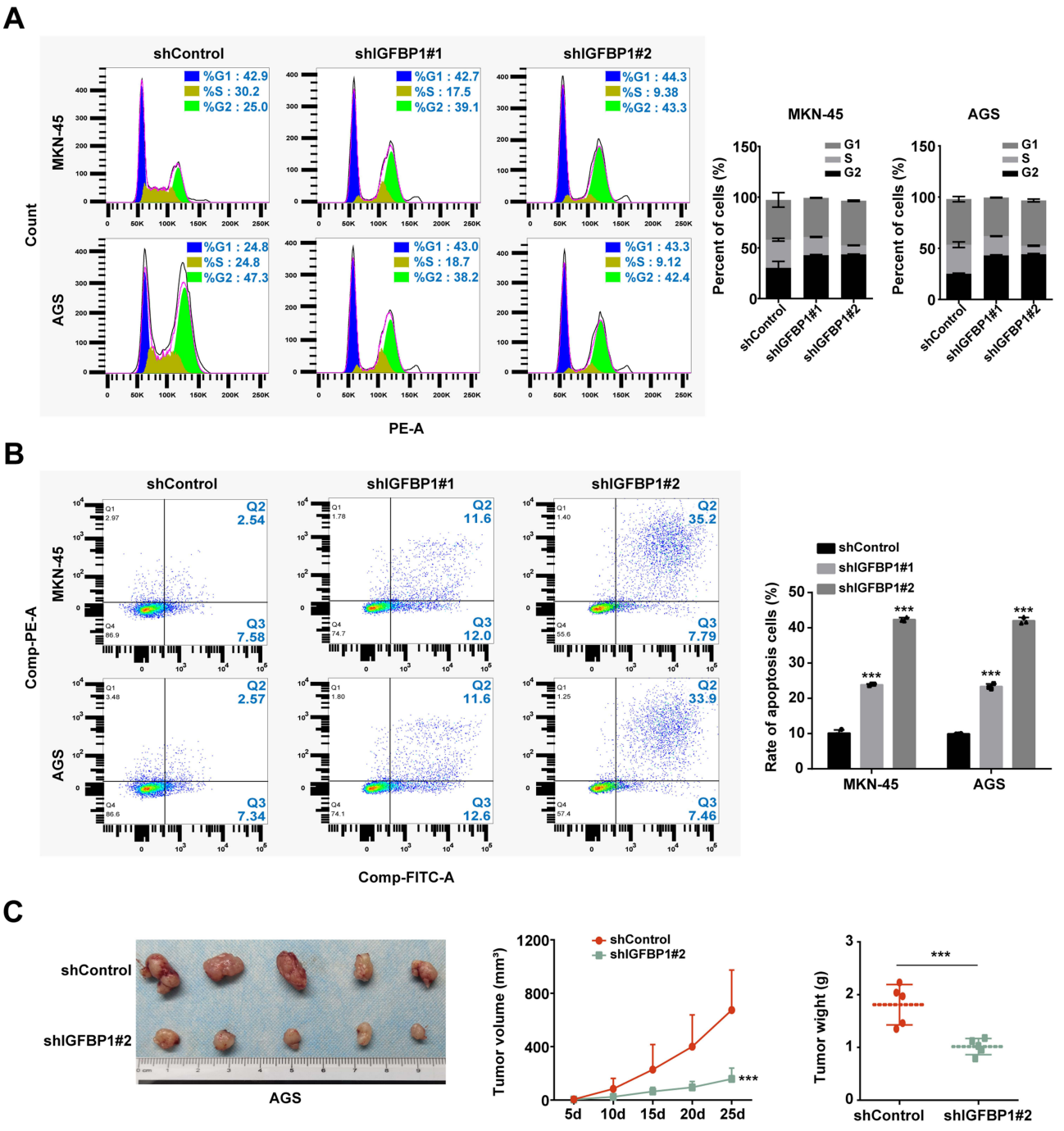

Figure 6 The effects of IGFBP1 on cell cycle and apoptosis in gastric cancer (GC) cells. (**A**) Flow cytometry was adopted to assess the impact of shIGFBP1 on the cell cycle of MKN45 and AGS cells (blue represents the G1 phase, yellow represents the S phase, and green represents the G2 phase). (**B**) Flow cytometry was used to assess the effect of shIGFBP1 on apoptosis in MKN45 and AGS cells. (**C**) Images of tumors excised from mice. MKN45 cells transfected with shIGFBP1 or shControl were injected subcutaneously into nude mice, respectively. Measure tumor volumes at five-day intervals following the injection, and tumors were finally collected for photography and weighing. Data were reported as the mean ± standard deviation (SD) from at least three independent trials. ***P<0.001.

containing F7 and topotecan as an advanced nano-drug delivery platform for tumor hyperthermia.[27] Ravi et al have provided evidence that inhibition of FAAH enhances the anti-tumor effects mediated by anandamide in non-small cell lung cancer by reducing the activity of the EGF/EGFR pathway.[28] Qian et al suggested that PSAT1 was a underlying prognostic factor for predicting clinical results in patients with colorectal carcinoma.[29] Significantly, we found that higher levels of IGFBP1 expression were linked to decreased rates of RFS and OS in individuals diagnosed with GC.

https://doi.org/10.2147/OTT.S499695

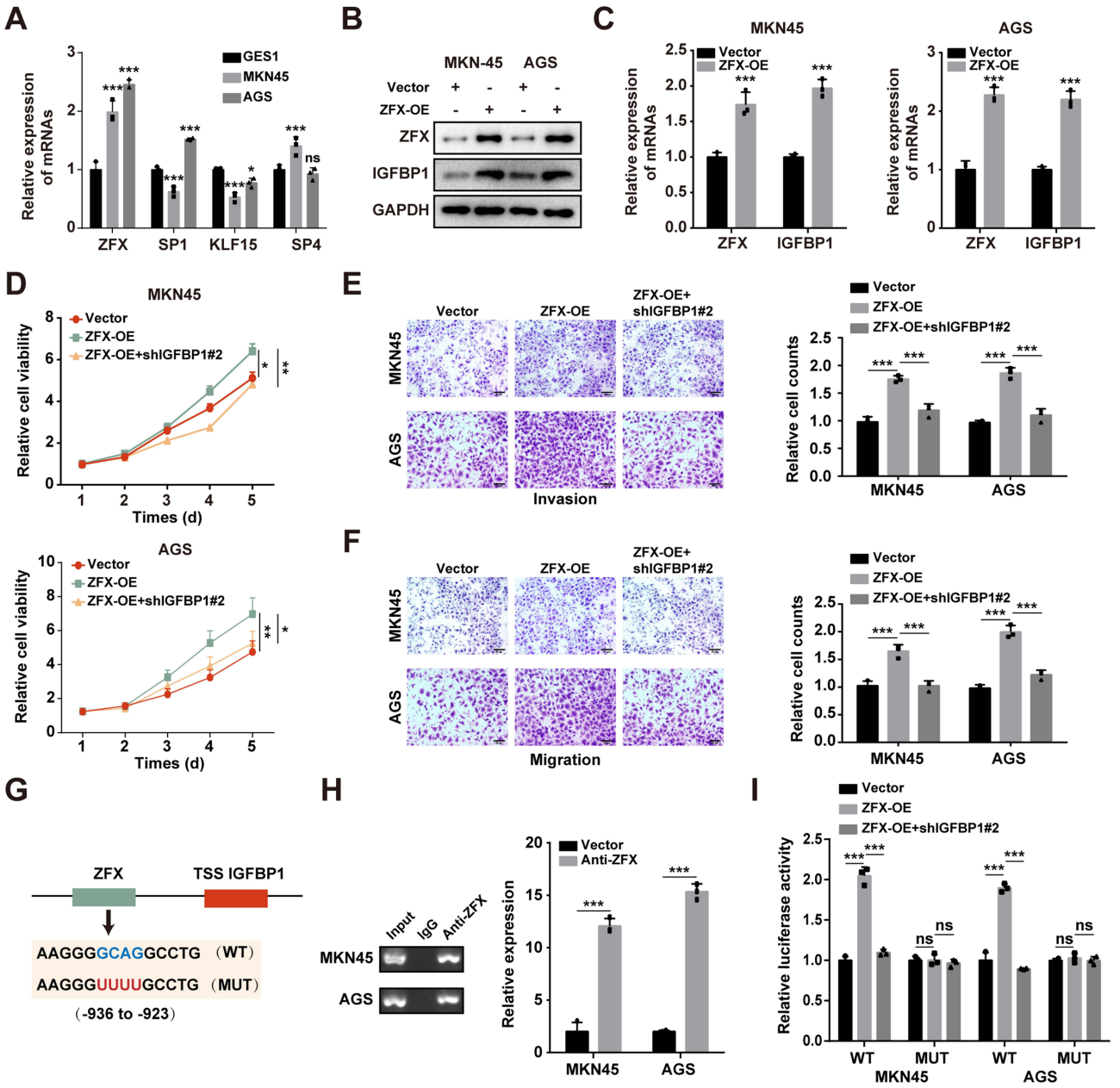

Figure 7 ZFX regulates the progression of gastric cancer (GC) cells by targeting IGFBP1. (**A**) Relative mRNA expression levels of ZFX, KLF15, SP1, and SP4 genes in GES1, MKN45, and AGS cell lines were detected by real-time quantitative polymerase chain reaction (RT-qPCR). (**B** and **C**) IGFBP1 expression levels in MKN45 and AGS cell lines under different treatment conditions (Vector control vs ZFX overexpression, ie, ZFX-OE) were examined by qRT-PCR (**B**) and Western blot analysis (**C**). (**D**) CCK-8 assays were performed to assess the proliferation of MKN45 or AGS cells infected with shControl, shIGFBP1, or shIGFBP1 combined with ZFX overexpression (ZFX-OE) at specified time points. Data are presented as mean ± standard deviation (SD) from at least three independent experiments. (**E** and **F**) MKN45 or AGS cells were infected with shControl, shIGFBP1, or shIGFBP1 combined with ZFX-OE. (**E**) Cell invasion ability was measured using Transwell migration assays; (**F**) Cell migration ability was determined using Transwell invasion assays. Data were reported as the mean ± standard deviation (SD) from at least three independent trials. (**G**) Bioinformatic algorithms were used to predict potential interaction sites between ZFX and the IGFBP1 gene, and the mutated sequences in the MUT vector are listed. (**H**) Chromatin immunoprecipitation (ChIP) analysis in MKN45 and AGS cells. Shown data are mean ± SD from three replicates. (**I**) Luciferase reporters containing the ZFX target sequence, including wild-type (WT) and corresponding mutant sequences (MUT), were constructed. WT and MUT reporters were co-transfected with shIGFBP1, and luciferase activity was measured. n.s. indicates no significant difference, *p < 0.05, **P<0.01, ***P<0.001.

IGFBP1, as a member of the secreted protein family, plays a pivotal role in modulating the biological activity of IGF-I, thereby exerting significant influence on various physiological functions of IGFs, including cell proliferation, survival, motility, and metabolism.[30] Many studies have reported that IGFBP1 inhibits the proliferation and migration of various human tumor cells in vitro.[21,31] Meanwhile, IGFBP1 can function as a carcinogenic gene, facilitating the migration of tumor cells and inducing drug resistance.[31,32] However, the exact function of IGFBP1 in GC and the underlying mechanisms remain

https://doi.org/10.2147/OTT.S499695

incompletely elucidated. In our study, we reveal the oncogenic role of IGFBP1 in GC by promoting the progression of GC cells. Moreover, the knockdown of IGFBP1 resulted in a significant reduction in the proliferation, invasion, and migration of GC cells. Similar results were observed in experiments in vivo. Hence, the results indicate that the involvement of IGFBP1 is crucial in the advancement of GC, thus highlighting its potential as a prospective target for therapeutic intervention in GC.

Previous studies have shown that ZFX is a key regulator of stem cells and human tumor development. For example, ZFX protein is crucially involved in governing the self-renewal process of both embryonic and hematopoietic stem cells.[33] Furthermore, ZFX is reportedly involved in the promotion of various cancer development and progression.[34,35] Importantly, ZFX can function as a transcription factors (TFs) to activate the transcription of downstream genes in various human tumors.[36] Likewise, this study has identified ZFX as a pivotal transcriptional activator of IGFBP1, a regulatory axis that has not been previously reported in gastric cancer. While prior research has established IGFBP1 as a prognostic marker for gastric cancer,[20] the involvement of ZFX provides a novel perspective on the overexpression of IGFBP1. Notably, the discovery of the ZFX-IGFBP1 axis opens up new avenues for therapeutic strategies targeting metabolic reprogramming. Future investigations could explore the synergistic effects of combining ZFX inhibition with existing chemotherapy regimens.

The present study, however, was subject to a few limitations. Firstly, the performance of the 10-metabolic gene prognostic signature remains to be validated in a larger GC sample. Secondly, the construction of the nomogram was based on data acquired from the TCGA database, which was involved in the underlying hazard of selection bias. Thirdly, more clinical variables should be included in the external validation set to elevate the prognostic prediction value of the 10-metabolic gene signature.

Conclusion

We successfully constructed a 10-metabolic gene signature and a metabolic gene-related nomogram to predict GC patients' RFS. We found that the 10-metabolic gene signature could be underlying prognostic classifier for GC patients. In addition, IGFBP1 act as an oncogene and can serve as a potential prognostic marker and gene therapy target for patients with GC.

Data Sharing Statement

The data that support the findings of this study are available from the corresponding author upon reasonable request.

Acknowledgment

Hui Liu and Yongming Huang are co-first authors for this study. The authors sincerely appreciate all lab members.

Author Contributions

All authors made a significant contribution to the work reported, whether that is in the conception, study design, execution, acquisition of data, analysis and interpretation, or in all these areas; took part in drafting, revising or critically reviewing the article; gave final approval of the version to be published; have agreed on the journal to which the article has been submitted; and agree to be accountable for all aspects of the work.

Funding

This project was supported by National Natural Science Foundation of China (82000512), Hubei Provincial Natural Science Foundation (Grant No. JCZRYB202501468) and The Scientific Research Fund of Union Hospital, Tongji Medical College, Huazhong University of Science and Technology (No. 2024-33).

Disclosure

The authors report no conflicts of interest in this work.

References

1. Zou J, Xu Y. MicroRNA-140 inhibits cell proliferation in gastric cancer cell line HGC-27 by suppressing SOX4. *Med Sci Monit*. 2016;22:2243–2252. doi:10.12659/MSM.896633
2. Zhang M, Dong BB, Lu M, et al. miR-429 functions as a tumor suppressor by targeting FSCN1 in gastric cancer cells. *Onco Targets Ther*. 2016;9:1123–1133. doi:10.2147/OTT.S91879
3. Zhu M, Zhou X, Du Y, et al. miR-20a induces cisplatin resistance of a human gastric cancer cell line via targeting CYLD. *Mol Med Rep*. 2016;14 (2):1742–1750. doi:10.3892/mmr.2016.5413
4. Zhuang K, Han K, Tang H, et al. Up-regulation of plasma miR-23b is associated with poor prognosis of gastric cancer. *Med Sci Monit*. 2016;22:356–361. doi:10.12659/MSM.895428
5. Strong VE, Wu A-W, Selby LV, et al. Differences in gastric cancer survival between the U.S. and China. *J Surg Oncol*. 2015;112(1):31–37. doi:10.1002/jso.23940
6. Zong L, Abe M, Seto Y, et al. The challenge of screening for early gastric cancer in China. *Lancet*. 2016;388(10060):2606. doi:10.1016/S0140-6736(16)32226-7
7. Massague J, Obenauf AC. Metastatic colonization by circulating tumour cells. *Nature*. 2016;529(7586):298–306. doi:10.1038/nature17038
8. Mlecnik B, Bindea G, Kirilovsky A, et al. The tumor microenvironment and Immunoscore are critical determinants of dissemination to distant metastasis. *Sci Transl Med*. 2016;8(327):327ra26. doi:10.1126/scitranslmed.aad6352
9. Xie SS, Jin J, Xu X, Zhuo W, Zhou TH. Emerging roles of non-coding RNAs in gastric cancer: pathogenesis and clinical implications. *World J Gastroenterol*. 2016;22(3):1213–1223. doi:10.3748/wjg.v22.i3.1213
10. Wu C, Zheng X, Li X, et al. Reduction of gastric cancer proliferation and invasion by miR-15a mediated suppression of Bmi-1 translation. *Oncotarget*. 2016;7(12):14522–14536. doi:10.18632/oncotarget.7392
11. Wang Y, Zeng J, Pan J, et al. MiR-320a inhibits gastric carcinoma by targeting activity in the FoxM1-P27KIP1 axis. *Oncotarget*. 2016;7 (20):29275–29286. doi:10.18632/oncotarget.8676
12. Wang LL, Zhang XH, Zhang X, et al. MiR-30a increases cisplatin sensitivity of gastric cancer cells through suppressing epithelial-to-mesenchymal transition (EMT). *Eur Rev Med Pharmacol Sci*. 2016;20(9):1733–1739.
13. Pavlova NN, Thompson CB. The Emerging Hallmarks of Cancer Metabolism. *Cell Metab*. 2016;23(1):27–47. doi:10.1016/j.cmet.2015.12.006
14. Jain M, Nilsson R, Sharma S, et al. Metabolite profiling identifies a key role for glycine in rapid cancer cell proliferation. *Science*. 2012;336 (6084):1040–1044. doi:10.1126/science.1218595
15. Sun R, Bao M-Y, Long X, et al. Metabolic gene NR4A1 as a potential therapeutic target for non-smoking female non-small cell lung cancer patients. *Thorac Cancer*. 2019;10(4):715–727. doi:10.1111/1759-7714.12989
16. Nwosu ZC, Battello N, Rothley M, et al. Liver cancer cell lines distinctly mimic the metabolic gene expression pattern of the corresponding human tumours. *J Exp Clin Cancer Res*. 2018;37(1):211. doi:10.1186/s13046-018-0872-6
17. Na KJ, Choi H. Tumor metabolic features identified by (18)F-FDG PET correlate with gene networks of immune cell microenvironment in head and neck cancer. *J Nucl Med*. 2018;59(1):31–37. doi:10.2967/jnumed.117.194217
18. Yao L, Wang L, Cao Z-G, et al. High expression of metabolic enzyme PFKFB4 is associated with poor prognosis of operable breast cancer. *Cancer Cell Int*. 2019;19(1):165. doi:10.1186/s12935-019-0882-2
19. Gajjar KK, Vora HH, Kobawala TP, et al. Deciphering the potential value of 5-fluorouracil metabolic enzymes in predicting prognosis and treatment response of colorectal cancer patients. *Int J Biol Markers*. 2018;33(2):180–188. doi:10.1177/1724600817748539
20. Liu Q, Jiang J, Zhang X, et al. Comprehensive analysis of IGFBPs as biomarkers in gastric cancer. *Front Oncol*. 2021;11:723131. doi:10.3389/fonc.2021.723131
21. Cai G, Qi Y, Wei P, et al. IGFBP1 sustains cell survival during spatially-confined migration and promotes tumor metastasis. *Adv Sci*. 2023;10(21): e2206540. doi:10.1002/advs.202206540
22. Colaprico A, Silva TC, Olsen C, et al. TCGAbiolinks: an R/Bioconductor package for integrative analysis of TCGA data. *Nucleic Acids Res*. 2016;44(8):e71. doi:10.1093/nar/gkv1507
23. Davis S, Meltzer PS. GEOquery: a bridge between the gene expression omnibus (GEO) and BIOCONDUCTOR. *Bioinformatics*. 2007;23 (14):1846–1847. doi:10.1093/bioinformatics/btm254
24. Bray F, Ferlay J, Soerjomataram I, et al. Global cancer statistics 2018: GLOBOCAN estimates of incidence and mortality worldwide for 36 cancers in 185 countries. *CA Cancer J Clin*. 2018;68(6):394–424. doi:10.3322/caac.21492
25. Casamayor M, Morlock R, Maeda H, et al. Targeted literature review of the global burden of gastric cancer. *Ecancermedicalscience*. 2018;12:883. doi:10.3332/ecancer.2018.883
26. Chai HJ, Ren Q, Fan Q, et al. PAX8 is a potential marker for the diagnosis of primary epithelial ovarian cancer. *Oncol Lett*. 2017;14(5):5871–5875. doi:10.3892/ol.2017.6949
27. Du C, Li S, Li Y, et al. F7 and topotecan co-loaded thermosensitive liposome as a nano-drug delivery system for tumor hyperthermia. *Drug Deliv*. 2020;27(1):836–847. doi:10.1080/10717544.2020.1772409
28. Ravi J, Sneh A, Shilo K, et al. FAAH inhibition enhances anandamide mediated anti-tumorigenic effects in non-small cell lung cancer by downregulating the EGF/EGFR pathway. *Oncotarget*. 2014;5(9):2475–2486. doi:10.18632/oncotarget.1723
29. Qian C, Xia Y, Ren Y, et al. Identification and validation of PSAT1 as a potential prognostic factor for predicting clinical outcomes in patients with colorectal carcinoma. *Oncol Lett*. 2017;14(6):8014–8020. doi:10.3892/ol.2017.7211
30. Baxter RC. IGF binding proteins in cancer: mechanistic and clinical insights. *Nat Rev Cancer*. 2014;14(5):329–341. doi:10.1038/nrc3720
31. Zhang B, Hong CQ, Lin YW, et al. Association between IGFBP1 expression and cancer risk: a systematic review and meta-analysis. *Heliyon*. 2023;9(6):1.
32. Tang Q, Zhou Q, Li J, et al. Solamargine enhanced gefitinib antitumor effect via regulating MALAT1/miR-141-3p/Sp1/IGFBP1 signaling pathway in non-small cell lung cancer. *Carcinogenesis*. 2023;44(6):497–510. doi:10.1093/carcin/bgad028
33. Chin W-C. ZFX controls the self-renewal of human embryonic stem cells. *PLoS One*. 2012;7(8):1.
34. Song X, Zhu M, Zhang F, et al. ZFX promotes proliferation and metastasis of pancreatic cancer cells via the MAPK pathway. *Cell Physiol Biochem*. 2018;48(1):274–284. doi:10.1159/000491727

35. Yang D, Ma X, Xu J, et al. Zfx-induced upregulation of UBE2J1 facilitates endometrial cancer progression via PI3K/AKT pathway. *Cancer Biol Ther*. 2021;22(3):238–247. doi:10.1080/15384047.2021.1883186
36. Rhie SK, Yao L, Luo Z, et al. ZFX acts as a transcriptional activator in multiple types of human tumors by binding downstream from transcription start sites at the majority of CpG island promoters. *Genome Res*. 2018;28(3):310–320. doi:10.1101/gr.228809.117